

# Cluster Morphologies as a Test of Different Cosmological Models

Tamon Suwa and Asao Habe

*Division of Physics, Graduate School of Science, Hokkaido University, Sapporo 060-0810,  
Japan*

[tamon@astro1.sci.hokudai.ac.jp](mailto:tamon@astro1.sci.hokudai.ac.jp)

[habe@astro1.sci.hokudai.ac.jp](mailto:habe@astro1.sci.hokudai.ac.jp)

Kohji Yoshikawa

*Department of Astronomy, Kyoto University, Kyoto 606-8502, Japan*

[kohji@kusastro.kyoto-u.ac.jp](mailto:kohji@kusastro.kyoto-u.ac.jp)

and

Takashi Okamoto

*Yukawa Institute for Theoretical Physics, Kyoto University, Kyoto 606-8502, Japan  
AND*

*Department of Physics, University of Durham, South Road, Durham, DH1 3LE, England*

[Takashi.Okamoto@durham.ac.uk](mailto:Takashi.Okamoto@durham.ac.uk)

## ABSTRACT

We investigate how cluster morphology is affected by the cosmological constant in low-density universes. Using high-resolution cosmological N-body/SPH simulations of flat ( $\Omega_0 = 0.3$ ,  $\lambda_0 = 0.7$ ,  $\Lambda$ CDM) and open ( $\Omega_0 = 0.3$ ,  $\lambda_0 = 0$ , OCDM) cold dark matter universes, we calculate statistical indicators to quantify the irregularity of the cluster morphologies. We study axial ratios, center shifts, cluster clumpiness, and multipole moment power ratios as indicators for the simulated clusters at  $z = 0$  and 0.5. Some of these indicators are calculated for both the X-ray surface brightness and projected mass distributions. In  $\Lambda$ CDM all these indicators tend to be larger than those in OCDM at  $z = 0$ . This result is consistent with the analytical prediction of Richstone, Loeb, & Turner, that is, clusters in  $\Lambda$ CDM are formed later than in OCDM, and have more substructure at  $z = 0$ . We make a Kolmogorov-Smirnov test on each indicator for these two

models. We then find that the results for the multipole moment power ratios and the center shifts for the X-ray surface brightness are under the significance level (5%). We results also show that these two cosmological models can be distinguished more clearly at  $z = 0$  than  $z = 0.5$  by these indicators.

*Subject headings:* galaxies:clusters:general – cosmology:theory – methods:numerical

## 1. INTRODUCTION

Measurement of the cosmological parameters, such as the Hubble constant  $H_0$ , the density parameter  $\Omega_0$ , and the cosmological constant  $\Lambda$ , is one of the most important studies in observational cosmology. From observational evidence, the density parameter  $\Omega_0$  is estimated to be around 0.3 (e.g. Bahcall et al. 1999). The inflationary cosmology requires  $\Omega_0 + \lambda_0 = 1$ , where  $\lambda_0 = \Lambda/(3H_0^2)$ , and is supported by recent observations of the cosmic microwave background (e.g. de Bernardis et al. 2000). Distant Type Ia supernovae (SNe Ia) are assumed to be standard candles to explore the effect of a cosmological constant by searching for evidence of accelerated expansion (Perlmutter et al. 1999; Riess et al. 1998). Several systematic uncertainties in the observational data of SNe Ia have been pointed out (Totani & Kobayashi 1999; Gibson et al. 2000). Therefore, independent studies in the non-linear regime are important to confirm the values of the cosmological parameters.

Richstone, Loeb, & Turner (1992) proposed that the fraction of clusters which have significant substructure can be a probe of the density parameter,  $\Omega_0$ , since the fraction of recently formed clusters strongly depends upon  $\Omega_0$  and such young clusters are likely to have substructure. They have also revealed that the formation epoch of clusters in a universe with a cosmological constant is later than that in a universe without a cosmological constant, although the effect of the cosmological constant is much smaller than that of the density parameter. In fact, Wilson, Cole, & Frenk (1996) showed that the statistics of the quadruples of the column mass density of clusters strongly depends on the value of  $\Omega_0$ , while it is quite insensitive to the value of  $\lambda_0$ .

Some authors have studied if cosmological models with and without a cosmological constant can be discriminated by the statistics of the irregularity of cluster morphologies (Jing et al. 1995; Crone, Evrard, & Richstone 1996; Buote & Xu 1997). They performed pure N-body simulations in low-density flat universes ( $\Omega_0 = 0.2\text{--}0.35$ ,  $\lambda_0 = 1 - \Omega_0$ ) and open universes ( $\Omega_0 = 0.2\text{--}0.35$ ,  $\lambda_0 = 0$ ). Jing et al. (1995) and Crone et al. (1996) quantified morphologies of X-ray surface brightness of clusters from the  $N$ -body results assuming hydrostatic equilibrium of the hot gas in the gravitational potentials of the clusters. Using

a Kolmogorov-Smirnov test (hereafter KS-test), they showed that a low-density flat universe and an open universe are distinguishable from each other by the center shifts. On the other hand, Buote & Xu (1997) obtained multipole moment power ratios for clusters in their N-body simulations and compared those in a low-density flat universe and an open universe. They concluded that these two cosmological models are not distinguishable by the multipole power ratios. Since these authors estimated the hot gas distribution from N-body simulations, their results are in question, and then simulations including hydrodynamics are desired.

In previous hydrodynamic simulations (Evrard et al. 1993; Mohr et al. 1995) the numbers of clusters were not enough to perform a statistical comparison. Although Valdarnini, Ghizzardi, & Bonometto (1999) analyzed a sufficient number of clusters for various cosmological models, the effect of the tidal field from larger scales ( $\gtrsim 30\text{--}50 h^{-1}\text{Mpc}$ ) was neglected in their simulations because they performed tree-SPH simulations of individual clusters selected from the large  $N$ -body simulations. By comparing the simulated clusters and the ROSAT X-ray cluster data, they pointed out that the statistical test for the observed data favors the high-density ( $\Omega_0 = 1$ , SCDM) model rather than the *concordant* low-density flat ( $\Omega_0 = 0.3$ ,  $\lambda_0 = 0.7$ ) model. It is worthwhile to confirm their results by simulations that take account of the tidal field from outside the clusters. We then simulate comoving  $150 h^{-1}\text{Mpc}$  boxes with particle-particle-particle-mesh (P<sup>3</sup>M)-Smoothed Particle Hydrodynamics (SPH) code.

In this paper, we study morphologies of simulated clusters in flat ( $\Omega_0 = 0.3$ ,  $\lambda_0 = 0.7$ ,  $\Lambda\text{CDM}$ ) and open ( $\Omega_0 = 0.3$ ,  $\lambda_0 = 0$ ,  $\text{OCDM}$ ) cold dark matter universes by using high resolution simulations. We perform large simulations to obtain a sufficient number of clusters for statistical comparisons. A reason why we study the difference between low-density universes despite the fact that recent CMB data (e.g. de Bernardis et al. 2000) supports a flat universe is as follows. As we mentioned above, the irregularity of cluster morphologies is quite sensitive to the value of  $\Omega_0$  while it is rather insensitive to the value of  $\lambda_0$ . Then the statistical indicators that can discriminate between the low-density models with and without the cosmological constant  $\lambda_0$  enable us to detect the small difference in the formation histories of clusters in different but similar cosmologies such as the low-density universe with a time dependent vacuum energy. Furthermore, because the CMB data provide us only the information about the linear density fluctuations, the consistency test in the non-linear regime is very important. For instance, if the finding of Valdarnini et al. (1999) is true, we should consider what causes the discrepancy. Unfortunately, the resolution in our simulations is not sufficient to make a direct comparison with high-resolution X-ray observations by Chandra or XMM and our simulations do not include some important physical processes like the cooling and heating, which may affect the morphology of the

X-ray surface brightness. Therefore here we restrict ourselves to finding effective statistical indicators to discriminate between two low-density universes and we do not compare our simulation results with the observations.

We identify clusters in our simulation and calculate various statistical indicators for them. The KS-tests are performed to measure how effectively these indicators distinguish between these two cosmological models. These indicators are calculated for the projected mass density as well as the X-ray surface brightness of clusters of galaxies. The X-ray surface brightness reflects the distribution of the hot gas in the cluster. On the other hand, the projected mass density is dominated by the distribution of dark matter. Although dark matter cannot be observed directly, a method by which the mass distribution is reconstructed from small distortion images of background galaxies caused by gravitational lensing (these small distortions are called the ‘weak shear field’) has been developed recently (e.g. Mellier 1999; Luppino & Kaiser 1997; Clowe et al. 2000). The precision of this method is not yet sufficient to probe cluster substructure. It is, however, likely that this mass reconstruction method will progress and become a useful tool to measure substructure in galaxy clusters. Schneider & Bartelmann (1997) have already investigated the possibility of deriving multipole moments of the projected mass distribution of clusters with weak-lensing.

The organization of this paper is as follows. In §2, we describe the numerical simulations used in this paper, the method of cluster identification, and the definitions of indicators which we use. We give mean values and standard deviations of the indicators for simulated clusters and show results of the KS-tests on these indicators in §3. In §4, we discuss our results and present our conclusion.

## 2. METHOD

### 2.1. Numerical Simulations

Our simulations are based on a P<sup>3</sup>M-SPH algorithm. Detailed description of our simulation method is given in Yoshikawa, Jing, & Suto (2000).

We use two cosmological models, OCDM and  $\Lambda$ CDM. Cosmological parameters in the two models, except for the cosmological constant, are as follows: the Hubble constant in units of  $100\text{km s}^{-1}\text{Mpc}^{-1}$ ,  $h = 0.7$ , the density parameter,  $\Omega_0 = 0.3$ , the baryon density parameter,  $\Omega_b = 0.015h^{-2}$ , the rms density fluctuation amplitude on a scale  $8h^{-1}\text{Mpc}$ ,  $\sigma_8 = 1.0$ , and the power-law index of the primordial density fluctuations,  $n = 1.0$ . The normalized cosmological constant,  $\lambda_0$  is 0 and 0.7 for OCDM and  $\Lambda$ CDM, respectively. The simulation of  $\Lambda$ CDM is the same as L150A in Yoshikawa et al. (2000) and that of OCDM is

carried out for this paper.

Each simulation employs  $N_{\text{DM}} = 128^3$  dark matter particles and the same number of SPH particles. The mass of a dark matter particle and an SPH particle are  $1.7 \times 10^{11} M_{\odot}$  and  $2.0 \times 10^{10} M_{\odot}$ , respectively. The size of comoving simulation box,  $L_{\text{box}}$ , is  $150h^{-1}\text{Mpc}$ , and the box has the periodic boundary conditions. We use the spline (S2) gravitational softening (Hockney & Eastwood 1981), and the softening length,  $\epsilon_{\text{grav}}$ , is set to be  $L_{\text{box}}/(10N_{\text{DM}}^{1/3})$  ( $\sim 120h^{-1}\text{kpc}$ ). The smoothing length of each SPH particle is determined by

$$h_i^{(n)} = \frac{1}{2} \left\{ 1 + \left( \frac{N_s}{N_i^{(n-1)}} \right)^{1/3} \right\} h_i^{(n-1)}, \quad (1)$$

where  $h_i^{(n)}$  is the smoothing length of the  $i$ -th particle at the  $n$ -th time step,  $N_i^{(n)}$  is the number of neighbor particles of the  $i$ -th particle at the  $n$ -th time step (the number of particles inside a sphere of radius  $h_i^{(n)}$ ), and  $N_s$  is mean number of neighbor particles (Hernquist & Katz 1989). We set  $N_s = 32$  and the minimum SPH smoothing length as  $h_{\text{min}} = \epsilon_{\text{grav}}/4$  ( $\sim 30h^{-1}\text{kpc}$ ). We use the COSMICS package (Bertschinger 1995) to generate initial conditions at  $z = 25$ . Our simulations are carried out on a VPP5000 and each run took about 50 hours using 8PE with parallel P<sup>3</sup>M-SPH. The memory resource needed to run each simulation is 500MB.

We calculate statistical indicators for the clusters in our simulations at  $z = 0.5$  and 0. The reason for this is that the formation rate of galaxy clusters in  $\Lambda\text{CDM}$  is expected to exceed that in  $\text{OCDM}$  for  $z < 0.8$  as shown in Fig.1 which shows the formation rate of galaxy clusters as a function of redshift according to the analytical formula given by Richstone et al. (1992). In Fig.1 the number of formed clusters is normalized by the present value and the cosmic time is also normalized by the present age of the universe. The solid and dashed curves indicate the formation rates in  $\Lambda\text{CDM}$  and in  $\text{OCDM}$ , respectively. Since just before  $z = 0.5$  the formation rate in  $\Lambda\text{CDM}$  exceeds that in  $\text{OCDM}$ , we expect that the difference due to the cosmological constant can already be detected at  $z = 0.5$ . Moreover, mass reconstruction based on observations of the weak shear field has an advantage for high-redshift clusters rather than nearby clusters in principle.

## 2.2. Cluster Identification

The way of identifying galaxy clusters is as follows (Jing & Fang 1994; Thomas et al. 1998).

1. We pick up SPH particles whose gas densities are more than 200 times the background

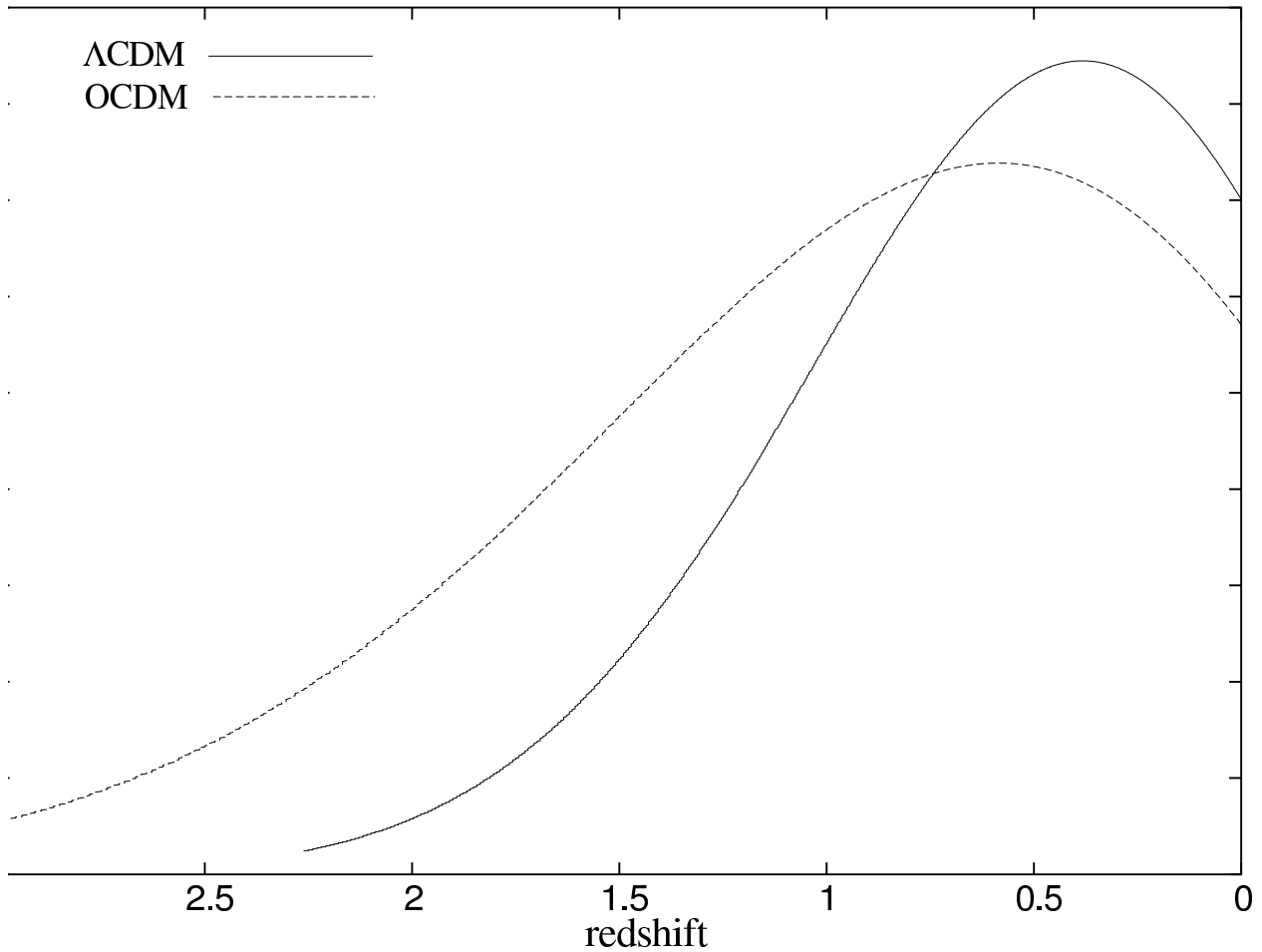


Fig. 1.— The formation rate of galaxy clusters. The solid curve indicates the formation rate in  $\Lambda$ CDM and the dashed curve indicates that in OCDM.

(gas and dark matter) density. Here, we define ‘gas density of an SPH particle’ as gas density at the position of the SPH particle. Processes at step 2 and 3 are performed for these selected particles.

2. We perform a Friends-of-Friends method (hereafter FoF; e.g. Davis et al. 1985) for the dense SPH particles selected by step 1. The linking length,  $l$ , is defined as  $b\bar{n}^{-1/3}$ , where  $\bar{n}$  is mean number density of all SPH and dark matter particles in the simulation box, and the constant parameter  $b = 0.5$ . It should be noted that the dense SPH particles are confined within small scale areas. Since the typical distance between these areas is significantly larger than  $l (= b\bar{n}^{-1/3})$ , the number of groups found by FoF does not depend on  $b$  strongly. We confirm that both the number of the groups found in this step and the number of clusters found in following steps are not so different for  $0.2 \leq b \leq 1.0$ .
3. The densest SPH particle in each group is defined as a ‘core’ particle of the group.
4. We draw a sphere of which the center is on the position of the ‘core’, and seek a radius in which the mean density of total matter is 200 times the background density of total matter. This radius is called  $r_{200}$ .
5. If the total mass in the sphere with radius  $r_{200}$  is more than  $2 \times 10^{14}h^{-1}M_{\odot}$ , a set of particles in the sphere is a candidate for being a cluster of galaxies.
6. If another ‘core’ particle exists in the sphere, the set which belongs to the less dense ‘core’ is removed from the cluster candidate list.

The candidates which are not removed finally are identified as clusters of galaxies. We define the center of a cluster by the position of the ‘core’ particle. We find that this position is very close to the particle having the minimum gravitational potential in the cluster and the distance between the ‘core’ particle and the potential minimum is at most several ten kpc in our simulation. We also find that the position of the ‘core’ is close to the center of mass of the cluster except for some clusters which have large substructures.

Fig.2 shows the mass distribution of the clusters. The upper panel describes the distribution in  $\Lambda$ CDM and the lower one describes the distribution in OCDM. The solid line indicates the number of clusters at  $z = 0$  and the dashed line indicates the number at  $z = 0.5$ . The maximum masses of clusters are  $2.7 \times 10^{15}h^{-1}M_{\odot}$  ( $\Lambda$ CDM,  $z = 0$ ),  $9.3 \times 10^{14}h^{-1}M_{\odot}$  ( $\Lambda$ CDM,  $z = 0.5$ ),  $2.7 \times 10^{15}h^{-1}M_{\odot}$  (OCDM,  $z = 0$ ), and  $1.2 \times 10^{15}h^{-1}M_{\odot}$  (OCDM,  $z = 0.5$ ). Table 1 shows the number of clusters found in each model. The numbers of clusters increase from  $z = 0.5$  to  $z = 0$ . Table 2 is the ratio of the mass inside clusters to the total mass in

the simulation box. These ratios in both models are similar to each other at  $z = 0$ , but the ratio in  $\Lambda$ CDM is smaller than that in OCDM at  $z = 0.5$ . This is consistent with the fact that  $\Lambda$ CDM clusters form later than OCDM clusters.

### 2.3. Calculation of Column Density and X-ray Surface Brightness

Two of the indicators we use in this paper, the center shifts and the power ratios, are calculated for X-ray surface brightness and the projected mass density for simulated clusters. Our numerical projection method from 3D to 2D is as follows.

At first, for each cluster, we prepare a cube centered on a core particle and the sides of the cube are set to  $2r_{200}$ . The total number of grid points in the cube is  $128^3$ . Each grid point is assigned indices  $(i, j, k)$  and this point is expressed by  $\mathbf{r}_{ijk}$ . We calculate gas density and temperature at each grid point from SPH particles in this cube. The gas density,  $\rho_{\text{gas}}$ , and temperature,  $T$ , at a grid point  $\mathbf{r}_{ijk}$  are given by

$$\rho_{\text{gas}}(\mathbf{r}_{ijk}) = \sum_s W(r_{s;ijk}/h_s) \frac{m_s}{h_s^3}, \quad (2)$$

$$T(\mathbf{r}_{ijk}) = \sum_s \frac{(\gamma - 1)\mu m_p}{k_B} W(r_{s;ijk}/h_s) u_s, \quad (3)$$

where  $h_s$ ,  $m_s$ ,  $u_s$ , and  $r_{s;ijk}$  are the  $s$ -th particle's smoothing length, mass, specific energy, and distance to the grid point ( $r_{s;ijk} = |\mathbf{r}_{ijk} - \mathbf{r}_s|$ , where  $\mathbf{r}_s$  is the position of the  $s$ -th particle), respectively.  $W(t)$  is an SPH kernel, which is defined as

$$W(t) \equiv \frac{1}{\pi} \begin{cases} 1 - (3/2)t^2 + (3/4)t^3 & \text{if } 0 \leq t \leq 1 \\ (2-t)^3/4 & \text{if } 1 \leq t \leq 2 \\ 0 & \text{otherwise.} \end{cases}$$

We assume the specific heat ratio  $\gamma = 5/3$  and the mean molecular mass  $\mu = 0.6$ . The smoothing length of an SPH particle is calculated in the usual way of the SPH method (Hernquist & Katz 1989; Monaghan 1992).

Model	z=0	z=0.5
$\Lambda$ CDM	66	28
OCDM	74	38

Table 1: The number of the clusters for each model and redshift.

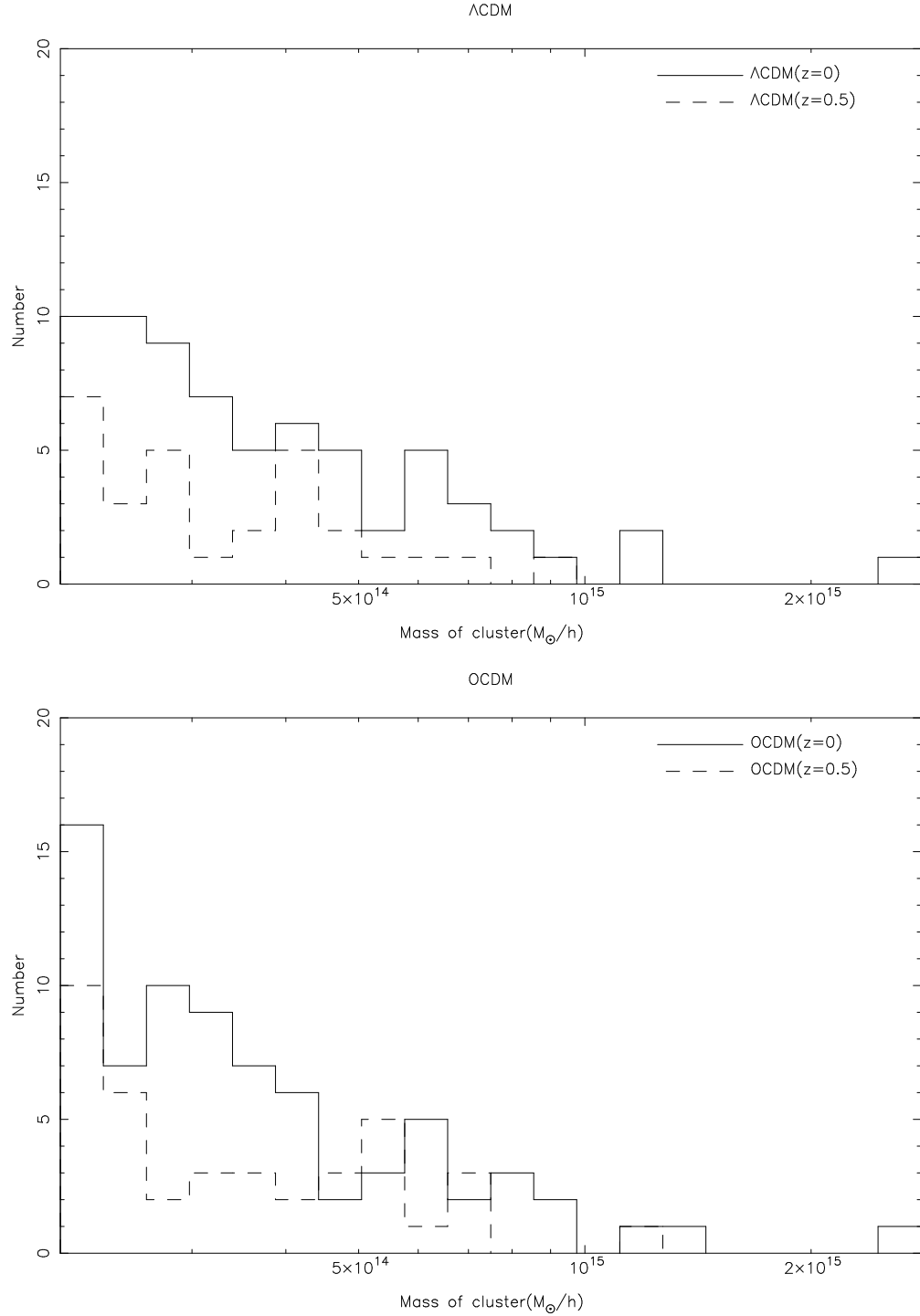


Fig. 2.— Mass distribution of the clusters. The upper panel describes the distribution in  $\Lambda$ CDM and the lower one describes the distribution in OCDM. The solid line indicates the number of clusters at  $z = 0$  and the dashed line indicates the number at  $z = 0.5$ .

In order to obtain the mass density at each grid point from dark matter particles in each cluster, we use an interpolation technique as in the previous SPH method. The smoothing length of each dark matter particle is set in order that each dark matter particle has  $32 \pm 3$  neighbors.

The column density,  $\sigma$ , is derived from the projection of the total mass density,  $\rho_{\text{dm}} + \rho_{\text{gas}}$ , where  $\rho_{\text{dm}}$  is dark matter density and  $\rho_{\text{gas}}$  is gas density. The X-ray surface brightness,  $\Sigma_X$ , is derived from the projection of  $\rho_{\text{gas}}^2 T^{1/2}$ .

## 2.4. Statistical Indicators

We calculate statistical indicators for each cluster of galaxies to quantify substructure and perform the KS-tests. As statistical indicators, we adopt the axial ratio, the  $M_{\text{int}}$ , the multipole moment power ratio, and the center shift. Definitions are described below.

### 2.4.1. Axial Ratio

The axial ratio is an indicator to show deviation from sphericity of a cluster of galaxies (Dutta 1995; Jing et al. 1995; Thomas et al. 1998). In a coordinate system whose origin is at the center of mass of the cluster, the following tensor's eigenvalues are calculated for all dark matter particles and SPH particles.

$$I_{ij} = \sum_s m_s x_i x_j. \quad (4)$$

These eigenvalues are labeled  $\lambda_1, \lambda_2, \lambda_3$  in decreasing order. If a cluster is an ellipsoid, its axial ratio is obtained by  $(\lambda_1/\lambda_3)^{1/2}$ .

Model	z=0	z=0.5
$\Lambda$ CDM	10.2%	3.64%
OCDM	11.4%	5.21%

Table 2: The ratios of the mass involved in the clusters to total mass in each simulation.

#### 2.4.2. $M_{\text{int}}$

We use  $M_{\text{int}}$  as an indicator of clumpiness of clusters. We calculate  $M_{\text{int}}$  in a similar way to Thomas et al. (1998). For each cluster we perform an FoF method for all dark matter particles and SPH particles with initial linking length,  $l = \bar{n}_c^{-1/3}$ , where  $\bar{n}_c$  is the mean number density of dark matter and SPH particles in the cluster. Next  $l$  is gradually lowered until  $l$  becomes  $(100\bar{n}_c)^{-1/3}$ . This causes the cluster to break up into several subclumps. At each stage  $M_{\text{int}}$  is defined as

$$M_{\text{int}} = \frac{m_1 + m_2 + m_3}{m_1}, \quad (5)$$

where  $m_1 \geq m_2 \geq m_3$  are masses of the three largest clumps. We use the maximum value of  $M_{\text{int}}$  as a measure of clumpiness of the cluster.

#### 2.4.3. *Center Shift*

The center shift measures major deviations from symmetry in the cluster mass distribution (Jing et al. 1995; Crone et al. 1996). We calculate the center shift for each cluster in a slightly different way from Jing et al. (1995). We first search for a peak value,  $c_{\text{peak}}$ , of  $\sigma$  or  $\Sigma_X$  in the cluster. The lowest contour level,  $c_{\text{lowest}}$ , is defined as the mean value of  $\sigma$  or  $\Sigma_X$  at  $0.5r_{200}$ . Next the  $i$ -th contour level is given as  $c_i \equiv c_{\text{peak}}(c_{\text{lowest}}/c_{\text{peak}})^{i/n_{\text{cont}}}$ , where  $n_{\text{cont}}$  is the total number of contours.

The center shift,  $C$ , is defined as

$$C = \sum_{i=1}^{n_{\text{cont}}} w_i \left\{ (x_i - \bar{x})^2 + (y_i - \bar{y})^2 \right\}, \quad (6)$$

where  $(x_i, y_i)$  is the center of the  $i$ -th contour, and  $\bar{x} = \sum_i w_i x_i$ , and  $\bar{y} = \sum_i w_i y_i$ . The weight of each contour,  $w_i$ , is proportional to the surface integral of  $\sigma$  or  $\Sigma_X$  in the region between this contour and the adjacent outer contour. The center shift shows the emission-weighted dispersion of the centers of contours. If a cluster has a lot of substructure, then the outer contour's center is expected to shift from  $(\bar{x}, \bar{y})$  and the center shift becomes large.

#### 2.4.4. *Power Ratio*

The power ratios quantify the shape of projected cluster potentials and are derived from their multipole expansions (e.g. Buote & Tsai 1995, 1996; Buote 1998; Valdarnini et al. 1999).

The two-dimensional potential,  $\Psi(R, \phi)$ , and column density,  $\sigma(R, \phi)$ , are related by Poisson's equation,

$$\nabla^2 \Psi(R, \phi) = \sigma(R, \phi), \quad (7)$$

where  $R$  and  $\phi$  are projected polar coordinates about the center of mass of the cluster, and we ignore the constant factor in equation(7). The multipole expansion of  $\Psi(R, \phi)$  which relies on the distribution of the material interior to  $R$  (e.g. Buote & Tsai 1995) is

$$\begin{aligned} \Psi(R, \phi) = & -a_0 \ln \left( \frac{1}{R} \right) - \sum_{m=1}^{\infty} \frac{1}{m R^m} \\ & \times (a_m \cos m\phi + b_m \sin m\phi), \end{aligned} \quad (8)$$

where  $a_m$  and  $b_m$  are defined as follows:

$$a_m = \int_{R' \leq R} \sigma(\mathbf{x}') (R')^m \cos m\phi' d^2 \mathbf{x}' \quad (9)$$

and

$$b_m = \int_{R' \leq R} \sigma(\mathbf{x}') (R')^m \sin m\phi' d^2 \mathbf{x}', \quad (10)$$

where  $\mathbf{x}' = (R', \phi')$ . The  $m$ -th moment power,  $P_m$ , is defined by integration of the square of the  $m$ -th term of the multipole expansion, equation (8), over the boundary of a circular aperture of radius  $R_{ap}$ ,

$$P_m = \frac{1}{2m^2 R_{ap}^{2m}} (a_m^2 + b_m^2) \quad (11)$$

for  $m > 0$ , and

$$P_0 = a_0^2 \quad (12)$$

for  $m = 0$ .

The moment power depends on not only the irregularity of the potential shape but also the magnitude of  $\sigma$ . Thus we use the moment power ratio,  $P_m/P_0$ , as an indicator of a cluster's irregularity. We define the unit of  $R$ , the radius in polar coordinates, as  $r_{200}$ , so that the power ratio is independent of the size of the cluster. Since the origin of the polar coordinates is the center of mass of the cluster, the dipole moment,  $P_1$ , is vanished. The higher order ( $m > 4$ , in this paper) terms are affected by minor irregularities in cluster shapes, hence we calculate the power ratio for only  $m = 2, 3$ , and 4. Because the power ratios depend on  $R_{ap}$  (Buote & Xu 1997; Valdarnini et al. 1999), we calculate the power ratios for some different values of  $R_{ap}$ .

We also use the same definition of the power ratio for  $\Sigma_X$  by replacing  $\sigma$  with  $\Sigma_X$  in equations (9) and (10).

### 3. RESULTS

According to the analytical results of Richstone et al. (1992), the typical formation epoch of galaxy clusters in  $\Lambda$ CDM is delayed to lower redshift than in OCDM. This delay clearly appears at low- $z$  ( $z \lesssim 0.8$ –0.7, as shown in Fig.1). We then calculate the indicators described in §2 at  $z = 0$  and  $z = 0.5$  and perform the KS-test for each set of indicators obtained for two cosmological models. The KS-test can be used as a statistical test to estimate the ability of an indicator to be used to discriminate between the model with and without  $\lambda_0$ . The result of the KS-test is the probability of the null-hypothesis that two distributions of the indicator are generated from the same population (Press et al. 1988). The significance level of the KS-test adopted in this paper is 5%. If the result of the KS-test for an indicator is under this level, we regard that it is able to distinguish two cosmological models by using these indicator.

#### 3.1. Axial Ratio

The mean values of the axial ratios are shown in Table 3. From  $z = 0.5$  to  $z = 0$  the axial ratio decreases. At  $z = 0$ , the axial ratio in  $\Lambda$ CDM is larger than in OCDM. This suggests that the clusters in  $\Lambda$ CDM have more substructures than in OCDM as expected from the analytical prediction.

The results of the KS-tests for axial ratios are 0.495 for  $z = 0$  and 0.661 for  $z = 0.5$ . Both are over the significance level(5%). Thus the axial ratio is not useful to distinguish these two cosmological models.

Jing et al. (1995) performed KS-test for axial ratios, which were obtained in a slightly different way to us, and the result of their KS-test is under the significance level ( $0.13 \times 10^{-2}$ ). In their calculations of principal axes and axial ratios, they take, at first, all particles within the virial radius of a cluster. They then calculate new principal axes and axial ratios using particles within an ellipsoid with the principal axes and axial ratios just determined. They repeat the same calculation for the updated ellipsoid until the axial ratios converge. We also

redshift	$\Lambda$ CDM	OCDM
$z = 0$	1.608	1.585
$z = 0.5$	1.644	1.696

Table 3: The mean values of the axial ratio.

calculate axial ratios by their method and perform a KS-test on them. In contrast with their result, the result of our KS-test is over the significance level (0.150 for  $z = 0$  and 0.750 for  $z = 0.5$ ) though our resolution is similar to theirs. The reason of this difference is unclear.

### 3.2. $M_{\text{int}}$

The mean values of  $M_{\text{int}}$  are shown in Table 4.  $M_{\text{int}}$  in  $\Lambda\text{CDM}$  is larger than that in  $\text{OCDM}$  at  $z = 0$ .

The results of the KS-tests for  $M_{\text{int}}$  are 0.770 for  $z = 0$  and 0.192 for  $z = 0.5$ . Both of them are over the significance level. Again we can not use this indicator to distinguish between these two cosmological models.

The mean values and the results of KS-tests are consistent with those of Thomas et al. (1998).

### 3.3. Center Shift

The mean values and the standard deviations of the logarithm of the center shifts are shown in Table 5. The number of the contours,  $n_{\text{cont}}$ , is varied from 4 to 8 to investigate the effect of the number of the contours. For large  $n_{\text{cont}}$ , i.e. a small interval of contour level,  $C$  is large. In the case of a small interval, the center shift easily shows small substructure near to the center of the cluster.

The center shifts for  $\sigma$ ,  $C_\sigma$ , are significantly larger than those for  $\Sigma_X$ ,  $C_{\Sigma_X}$ . The shapes of the  $\Sigma_X$  contours reflect the distribution of the gas. Gas in a cluster relaxes more quickly than the collisionless dark matter (Frenk et al. 1999). This is the reason why the shapes of the  $\Sigma_X$  contours become rounder than those of  $\sigma$  and the center shifts for  $\Sigma_X$  become smaller than those for  $\sigma$ .

The center shifts in  $\Lambda\text{CDM}$  are larger than those in  $\text{OCDM}$  at the same redshift. This

redshift	$\Lambda\text{CDM}$	$\text{OCDM}$
$z = 0$	1.289	1.188
$z = 0.5$	1.284	1.189

Table 4: The mean value of the  $M_{\text{int}}$ .

Model	$n_{\text{cont}}$	$\log(C_\sigma)$	$\log(C_{\Sigma_X})$
$\Lambda$ CDM			
$(z = 0)$	4	$-2.65(\pm 0.72)$	$-3.43(\pm 0.78)$
	5	$-2.52(\pm 0.69)$	$-3.31(\pm 0.82)$
	6	$-2.43(\pm 0.67)$	$-3.26(\pm 0.80)$
	7	$-2.38(\pm 0.64)$	$-3.22(\pm 0.80)$
	8	$-2.33(\pm 0.63)$	$-3.20(\pm 0.77)$
OCDM			
$(z = 0)$	4	$-2.80(\pm 0.70)$	$-3.64(\pm 0.75)$
	5	$-2.72(\pm 0.66)$	$-3.56(\pm 0.77)$
	6	$-2.62(\pm 0.67)$	$-3.49(\pm 0.75)$
	7	$-2.59(\pm 0.63)$	$-3.47(\pm 0.76)$
	8	$-2.54(\pm 0.62)$	$-3.46(\pm 0.76)$
$\Lambda$ CDM			
$(z = 0.5)$	4	$-2.87(\pm 0.58)$	$-3.73(\pm 0.67)$
	5	$-2.71(\pm 0.60)$	$-3.62(\pm 0.64)$
	6	$-2.67(\pm 0.57)$	$-3.53(\pm 0.64)$
	7	$-2.63(\pm 0.55)$	$-3.49(\pm 0.67)$
	8	$-2.59(\pm 0.55)$	$-3.45(\pm 0.64)$
OCDM			
$(z = 0.5)$	4	$-2.99(\pm 0.68)$	$-3.68(\pm 0.77)$
	5	$-2.89(\pm 0.70)$	$-3.59(\pm 0.80)$
	6	$-2.77(\pm 0.68)$	$-3.53(\pm 0.76)$
	7	$-2.73(\pm 0.70)$	$-3.46(\pm 0.76)$
	8	$-2.68(\pm 0.69)$	$-3.41(\pm 0.80)$

Table 5: Mean values of logarithm of center shifts

---

Note. — The first column indicates cosmological model and redshift. The second column shows the number of contours. The third and fourth columns are mean value of  $\log(C)$  for the column density and the X-ray surface brightness, respectively.

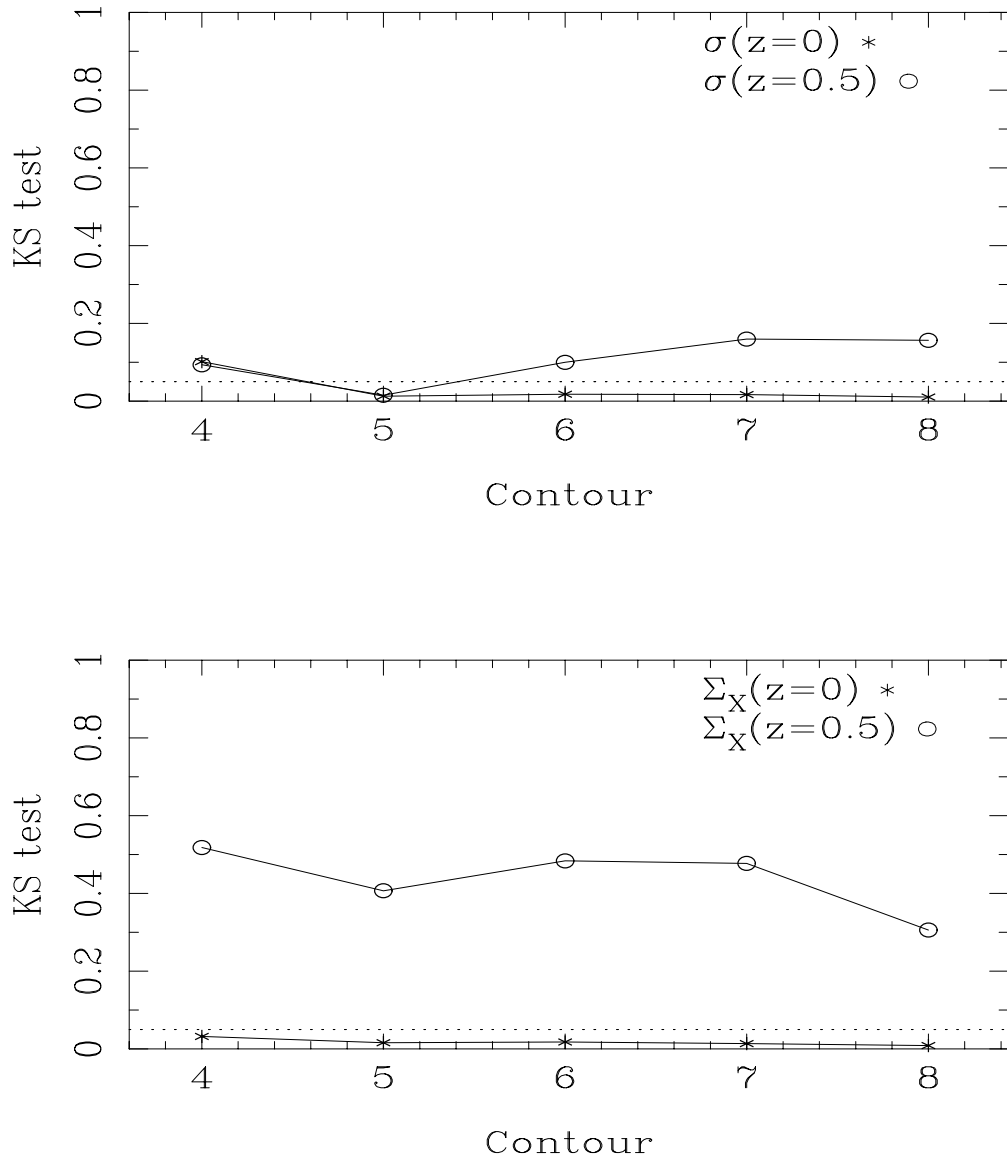


Fig. 3.— The results of the KS-tests for center shifts as a function of the number of contours. Asterisks indicate the results at  $z = 0$ , and circles indicate the results at  $z = 0.5$ . The dotted line describes the significance level(5%)

result reflects that the formation epoch of clusters in  $\Lambda$ CDM is later than in OCDM.

Fig.3 shows the result of the KS-tests for the center shifts. The upper panel describes the results for the center shifts for the column density and the lower one describes the results for the X-ray surface brightness. In Fig.3 the dotted line indicates the significance level(5%), asterisks indicate the results at  $z = 0$ , and circles indicate the results at  $z = 0.5$ . Using the center shifts for  $\Sigma_X$  at  $z = 0$ , we can distinguish the two cosmological models in this range of number of contours. The effect of contour level interval is not very significant for the KS-test.

In order to study the effect of the lowest level of contour, we also calculate the center shifts for  $\Sigma_X$  and  $\sigma$  in the two cases that the lowest contour level is the mean value at  $0.4r_{200}$  and  $0.7r_{200}$ . For the case of  $0.7r_{200}$ , the results of the KS-tests are over the significance level, except for one case with  $C_{\Sigma_X}$  ( $z=0$ ,  $n_{\text{cont}} = 8$ ). For the case of  $0.4r_{200}$ , the results are similar to the case of the lowest level at  $0.5r_{200}$ . We conclude that the center shift within  $\sim 0.5r_{200}$  is a useful tool to clarify the presence of a cosmological constant.

### 3.4. Power Ratio

We calculate the power ratios for various  $R_{ap}$  (0.4, 0.5, 0.6, 0.8, and 1.0 times  $r_{200}$ ) in order to study how  $R_{ap}$  affects the result of the KS-test. We show the mean values and the standard deviations of the logarithm of the power ratios in Tables 6 and 7, for the column density and the X-ray surface brightness, respectively. For small  $R_{ap}$ , the power ratios are large as shown in Table 6 and 7. The most likely explanation of this property is that the power ratios for small  $R_{ap}$  readily reflect the small substructures around the cluster center.

We also calculate the power ratios for constant  $R_{ap}$ , e.g.  $0.4h^{-1}\text{Mpc}$ , and  $0.6h^{-1}\text{Mpc}$ . As shown in Table 8, the power ratios for the constant  $R_{ap}$  are smaller than the proportional  $R_{ap}$  case because the constant  $R_{ap}$  is less sensitive to the small substructures in small clusters than is the proportional  $R_{ap}$ . In the constant  $R_{ap}$  case, the mean values and the standard deviations of the power ratios agree with Valdarnini et al. (1999).

From  $z = 0.5$  to  $z = 0$  the power ratios become smaller in both models. This is due to the fact that the fraction of relaxed clusters increases with time. Like the other indicators, the power ratios in  $\Lambda$ CDM are larger than those in OCDM at the same redshift as expected.

Table 9 shows the results of the KS-tests for the power ratios for the column density, and Table 10 shows those for the X-ray surface brightness. The figures with asterisks in these tables mean that they are under the significance level (5%). Figures 4–6 show the

Model	$R_{ap}$	$\log(P_2/P_0)$	$\log(P_3/P_0)$	$\log(P_4/P_0)$
$\Lambda$ CDM				
$(z = 0)$	$0.4r_{200}$	$-2.90(\pm 0.66)$	$-4.38(\pm 0.69)$	$-4.89(\pm 0.75)$
	$0.5r_{200}$	$-2.94(\pm 0.63)$	$-4.52(\pm 0.71)$	$-4.91(\pm 0.66)$
	$0.6r_{200}$	$-2.98(\pm 0.61)$	$-4.61(\pm 0.68)$	$-4.96(\pm 0.66)$
	$0.8r_{200}$	$-3.05(\pm 0.66)$	$-4.63(\pm 0.69)$	$-5.05(\pm 0.72)$
	$1.0r_{200}$	$-3.15(\pm 0.68)$	$-4.70(\pm 0.67)$	$-5.20(\pm 0.74)$
OCDM				
$(z = 0)$	$0.4r_{200}$	$-3.03(\pm 0.63)$	$-4.58(\pm 0.79)$	$-5.11(\pm 0.81)$
	$0.5r_{200}$	$-3.09(\pm 0.68)$	$-4.63(\pm 0.74)$	$-5.11(\pm 0.80)$
	$0.6r_{200}$	$-3.15(\pm 0.76)$	$-4.61(\pm 0.76)$	$-5.10(\pm 0.84)$
	$0.8r_{200}$	$-3.20(\pm 0.65)$	$-4.72(\pm 0.75)$	$-5.22(\pm 0.80)$
	$1.0r_{200}$	$-3.29(\pm 0.65)$	$-4.85(\pm 0.79)$	$-5.36(\pm 0.76)$
$\Lambda$ CDM				
$(z = 0.5)$	$0.4r_{200}$	$-2.93(\pm 0.69)$	$-4.33(\pm 0.67)$	$-4.88(\pm 0.69)$
	$0.5r_{200}$	$-2.92(\pm 0.51)$	$-4.37(\pm 0.58)$	$-4.89(\pm 0.65)$
	$0.6r_{200}$	$-2.92(\pm 0.50)$	$-4.40(\pm 0.57)$	$-4.85(\pm 0.66)$
	$0.8r_{200}$	$-2.91(\pm 0.51)$	$-4.35(\pm 0.51)$	$-4.85(\pm 0.67)$
	$1.0r_{200}$	$-2.93(\pm 0.51)$	$-4.39(\pm 0.63)$	$-4.81(\pm 0.64)$
OCDM				
$(z = 0.5)$	$0.4r_{200}$	$-2.76(\pm 0.52)$	$-4.29(\pm 0.93)$	$-4.78(\pm 0.86)$
	$0.5r_{200}$	$-2.78(\pm 0.52)$	$-4.38(\pm 0.93)$	$-4.75(\pm 0.80)$
	$0.6r_{200}$	$-2.80(\pm 0.54)$	$-4.40(\pm 0.90)$	$-4.79(\pm 0.82)$
	$0.8r_{200}$	$-2.87(\pm 0.61)$	$-4.43(\pm 0.77)$	$-4.90(\pm 0.96)$
	$1.0r_{200}$	$-3.02(\pm 0.64)$	$-4.44(\pm 0.73)$	$-5.02(\pm 0.94)$

Table 6: Mean values of  $\log(P_m/P_0)$  for column density

---

Note. — The first column describes cosmological models and redshifts. The upper two blocks are the data at  $z = 0$  and the lower two blocks are at  $z = 0.5$ . The Second column is aperture radius. The third to fifth columns are the mean values of power ratios of second, third, and fourth order, respectively.

Model	$R_{ap}$	$\log(P_2/P_0)$	$\log(P_3/P_0)$	$\log(P_4/P_0)$
$\Lambda$ CDM				
( $z = 0$ )	$0.4r_{200}$	$-3.92(\pm 0.96)$	$-5.86(\pm 1.14)$	$-6.52(\pm 1.31)$
	$0.5r_{200}$	$-4.19(\pm 0.99)$	$-6.16(\pm 1.14)$	$-6.81(\pm 1.32)$
	$0.6r_{200}$	$-4.40(\pm 1.01)$	$-6.36(\pm 1.22)$	$-7.03(\pm 1.34)$
	$0.8r_{200}$	$-4.75(\pm 1.05)$	$-6.66(\pm 1.32)$	$-7.37(\pm 1.41)$
	$1.0r_{200}$	$-5.04(\pm 1.09)$	$-6.93(\pm 1.40)$	$-7.67(\pm 1.49)$
OCDM				
( $z = 0$ )	$0.4r_{200}$	$-4.40(\pm 0.97)$	$-6.45(\pm 1.29)$	$-7.04(\pm 1.42)$
	$0.5r_{200}$	$-4.68(\pm 1.03)$	$-6.70(\pm 1.39)$	$-7.37(\pm 1.59)$
	$0.6r_{200}$	$-4.90(\pm 1.05)$	$-6.83(\pm 1.40)$	$-7.51(\pm 1.58)$
	$0.8r_{200}$	$-5.23(\pm 1.12)$	$-7.11(\pm 1.55)$	$-7.84(\pm 1.70)$
	$1.0r_{200}$	$-5.52(\pm 1.15)$	$-7.38(\pm 1.60)$	$-8.19(\pm 1.76)$
$\Lambda$ CDM				
( $z = 0.5$ )	$0.4r_{200}$	$-3.54(\pm 0.83)$	$-5.41(\pm 1.08)$	$-5.99(\pm 1.10)$
	$0.5r_{200}$	$-3.79(\pm 0.90)$	$-5.64(\pm 1.07)$	$-6.30(\pm 1.15)$
	$0.6r_{200}$	$-3.97(\pm 0.90)$	$-5.79(\pm 1.03)$	$-6.50(\pm 1.21)$
	$0.8r_{200}$	$-4.28(\pm 0.97)$	$-6.04(\pm 1.05)$	$-6.74(\pm 1.28)$
	$1.0r_{200}$	$-4.50(\pm 1.11)$	$-6.08(\pm 1.31)$	$-6.76(\pm 1.49)$
OCDM				
( $z = 0.5$ )	$0.4r_{200}$	$-3.63(\pm 1.16)$	$-5.35(\pm 1.53)$	$-6.03(\pm 1.64)$
	$0.5r_{200}$	$-3.87(\pm 1.20)$	$-5.59(\pm 1.59)$	$-6.26(\pm 1.75)$
	$0.6r_{200}$	$-4.04(\pm 1.21)$	$-5.83(\pm 1.66)$	$-6.45(\pm 1.79)$
	$0.8r_{200}$	$-4.29(\pm 1.35)$	$-6.05(\pm 1.77)$	$-6.71(\pm 2.05)$
	$1.0r_{200}$	$-4.59(\pm 1.40)$	$-6.30(\pm 1.87)$	$-6.98(\pm 2.08)$

Table 7: Mean values of  $\log(P_m/P_0)$  for X-ray surface brightness

Model	$R_{ap}$	$\log(P_2/P_0)$	$\log(P_3/P_0)$	$\log(P_4/P_0)$
$\Lambda$ CDM				
$(z = 0)$	$0.4h^{-1}\text{Mpc}$	$-5.65(\pm 0.85)$	$-7.66(\pm 1.14)$	$-8.22(\pm 1.23)$
	$0.6h^{-1}\text{Mpc}$	$-6.03(\pm 0.93)$	$-7.97(\pm 1.23)$	$-8.62(\pm 1.32)$
	$0.8h^{-1}\text{Mpc}$	$-6.39(\pm 0.98)$	$-8.39(\pm 1.14)$	$-8.98(\pm 1.31)$
	$1.0h^{-1}\text{Mpc}$	$-6.68(\pm 1.02)$	$-8.63(\pm 1.24)$	$-9.26(\pm 1.34)$
	$1.2h^{-1}\text{Mpc}$	$-6.90(\pm 1.05)$	$-8.81(\pm 1.31)$	$-9.52(\pm 1.45)$
$\text{OCDM}$				
$(z = 0)$	$0.4h^{-1}\text{Mpc}$	$-5.96(\pm 0.89)$	$-8.05(\pm 1.20)$	$-8.57(\pm 1.29)$
	$0.6h^{-1}\text{Mpc}$	$-6.47(\pm 0.96)$	$-8.55(\pm 1.21)$	$-9.09(\pm 1.40)$
	$0.8h^{-1}\text{Mpc}$	$-6.83(\pm 1.05)$	$-8.85(\pm 1.39)$	$-9.48(\pm 1.58)$
	$1.0h^{-1}\text{Mpc}$	$-7.12(\pm 1.08)$	$-9.07(\pm 1.47)$	$-9.74(\pm 1.64)$
	$1.2h^{-1}\text{Mpc}$	$-7.35(\pm 1.12)$	$-9.25(\pm 1.56)$	$-9.95(\pm 1.70)$
$\Lambda$ CDM				
$(z = 0.5)$	$0.4h^{-1}\text{Mpc}$	$-5.35(\pm 1.04)$	$-7.11(\pm 1.46)$	$-7.70(\pm 1.43)$
	$0.6h^{-1}\text{Mpc}$	$-5.78(\pm 1.20)$	$-7.57(\pm 1.54)$	$-8.22(\pm 1.69)$
	$0.8h^{-1}\text{Mpc}$	$-6.13(\pm 1.28)$	$-7.99(\pm 1.40)$	$-8.58(\pm 1.80)$
	$1.0h^{-1}\text{Mpc}$	$-6.36(\pm 1.33)$	$-8.17(\pm 1.48)$	$-8.68(\pm 1.81)$
	$1.2h^{-1}\text{Mpc}$	$-6.58(\pm 1.43)$	$-8.15(\pm 1.62)$	$-8.80(\pm 1.91)$
$\text{OCDM}$				
$(z = 0.5)$	$0.4h^{-1}\text{Mpc}$	$-5.58(\pm 1.21)$	$-7.28(\pm 1.64)$	$-7.95(\pm 1.74)$
	$0.6h^{-1}\text{Mpc}$	$-6.05(\pm 1.26)$	$-7.89(\pm 1.59)$	$-8.48(\pm 1.85)$
	$0.8h^{-1}\text{Mpc}$	$-6.39(\pm 1.35)$	$-8.12(\pm 1.75)$	$-8.74(\pm 2.03)$
	$1.0h^{-1}\text{Mpc}$	$-6.70(\pm 1.38)$	$-8.44(\pm 1.78)$	$-9.14(\pm 2.12)$
	$1.2h^{-1}\text{Mpc}$	$-6.94(\pm 1.39)$	$-8.67(\pm 1.80)$	$-9.34(\pm 1.99)$

Table 8: Mean values of  $\log(P_m/P_0)$  with constant  $R_{ap}$  for X-ray surface brightness.

results of the KS-tests summarized in Tables 9 and 10. At  $z = 0$ , we can distinguish the two cosmological models by the power ratios for  $\Sigma_X$  for all  $R_{ap}$ . Using the power ratios for  $\sigma$  for most  $R_{ap}$  except for  $P_3/P_0$ , we can also distinguish the two cosmological models.

#### 4. DISCUSSION AND CONCLUSIONS

We have investigated morphologies of the galaxy clusters in  $\Lambda$ CDM and OCDM at  $z = 0$  and  $z = 0.5$  using large hydrodynamic simulations. For clusters in each model we have calculated the axial ratios,  $M_{int}$ , center shifts, and multipole moment power ratios as statistical indicators that quantify the irregularity of cluster morphologies.

The power ratios and the center shifts are calculated for the projected density ( $\sigma$ ) as well as the X-ray surface brightness ( $\Sigma_X$ ). For  $\sigma$ , both indicators show a larger value than those for  $\Sigma_X$ , because the relaxation time scale of the collisionless particles is much longer than that of the collisional gas particles (Frenk et al. 1999; Valdarnini et al. 1999).

At  $z = 0$  all mean values of statistical indicators in  $\Lambda$ CDM show larger values than those in OCDM. These large values, which indicate large irregularity of the clusters, suggest more recent formation of the clusters in  $\Lambda$ CDM as expected from the analytic prediction (Richstone et al. 1992) and the previous numerical studies (Mohr et al. 1995; Crone et al. 1996; Buote & Xu 1997).

We use KS-tests to estimate the ability of the indicators to distinguish between two cosmological models. From the results of these KS-tests, the distributions of axial ratios in the two cosmological models are indistinguishable. The distributions of  $M_{int}$  in  $\Lambda$ CDM and OCDM are also similar. Using the center shifts and the power ratios for  $\Sigma_X$  at  $z = 0$ , we can distinguish the two cosmological models. It is possible to discriminate between  $\Lambda$ CDM and OCDM using the center shifts,  $P_2/P_0$ , and  $P_4/P_0$  for  $\sigma$  at  $z = 0$ . At  $z = 0.5$  we can distinguish the two cosmological models by the power ratios for  $\Sigma_X$ , but not by the center shifts for  $\Sigma_X$  or both the power ratios and the center shifts for  $\sigma$ .

Using the power ratios for  $\Sigma_X$  we can distinguish between  $\Lambda$ CDM and OCDM better than using those for  $\sigma$  as shown in Table 9 and 10. This may be due to the fact that the relaxation time scale of dark matter that dominates  $\sigma$  is longer than that of the gas on which  $\Sigma_X$  mainly depends, as described above. Since  $\sigma$  does not settle rapidly after the cluster formation epoch, the power ratios for  $\sigma$  are relatively insensitive to the difference of the cluster formation epochs.

We also note that the power ratios for  $\Sigma_X$  depend more on irregularities in high density

$P_m/P_0$	$R_{ap}$	$z = 0$	$z = 0.5$
$P_2/P_0$			
$0.4r_{200}$	2.43e-02*	4.45e-01	
$0.5r_{200}$	9.03e-02	4.57e-01	
$0.6r_{200}$	3.30e-02*	3.21e-01	
$0.8r_{200}$	1.38e-02*	6.84e-01	
$1.0r_{200}$	5.79e-03*	1.04e-01	
$P_3/P_0$			
$0.4r_{200}$	4.38e-02*	1.16e-01	
$0.5r_{200}$	1.23e-01	2.20e-01	
$0.6r_{200}$	3.37e-01	8.40e-02	
$0.8r_{200}$	4.28e-02*	4.87e-02*	
$1.0r_{200}$	1.24e-01	2.32e-01	
$P_4/P_0$			
$0.4r_{200}$	3.25e-02*	4.25e-01	
$0.5r_{200}$	1.40e-03*	3.60e-01	
$0.6r_{200}$	1.53e-02*	2.81e-01	
$0.8r_{200}$	1.43e-02*	1.36e-01	
$1.0r_{200}$	8.48e-02	8.97e-02	

Table 9: The results of the KS-tests for power ratios for the column density.

$P_m/P_0$	$R_{ap}$	$z = 0$	$z = 0.5$
$P_2/P_0$			
$0.4r_{200}$	4.19e-08*	1.03e-02*	
$0.5r_{200}$	7.20e-08*	1.47e-02*	
$0.6r_{200}$	1.33e-06*	2.70e-02*	
$0.8r_{200}$	1.47e-06*	2.99e-02*	
$1.0r_{200}$	2.56e-06*	3.30e-02*	
$P_3/P_0$			
$0.4r_{200}$	6.75e-06*	2.12e-01	
$0.5r_{200}$	3.51e-05*	1.42e-01	
$0.6r_{200}$	4.43e-05*	9.17e-03*	
$0.8r_{200}$	2.24e-03*	1.15e-03*	
$1.0r_{200}$	7.99e-04*	2.43e-03*	
$P_4/P_0$			
$0.4r_{200}$	2.06e-06*	1.79e-01	
$0.5r_{200}$	6.83e-05*	9.77e-02	
$0.6r_{200}$	4.72e-05*	3.22e-02*	
$0.8r_{200}$	2.52e-04*	1.28e-02*	
$1.0r_{200}$	7.56e-05*	2.68e-03*	

Table 10: The results of the KS-tests for power ratios for the X-ray surface brightness.

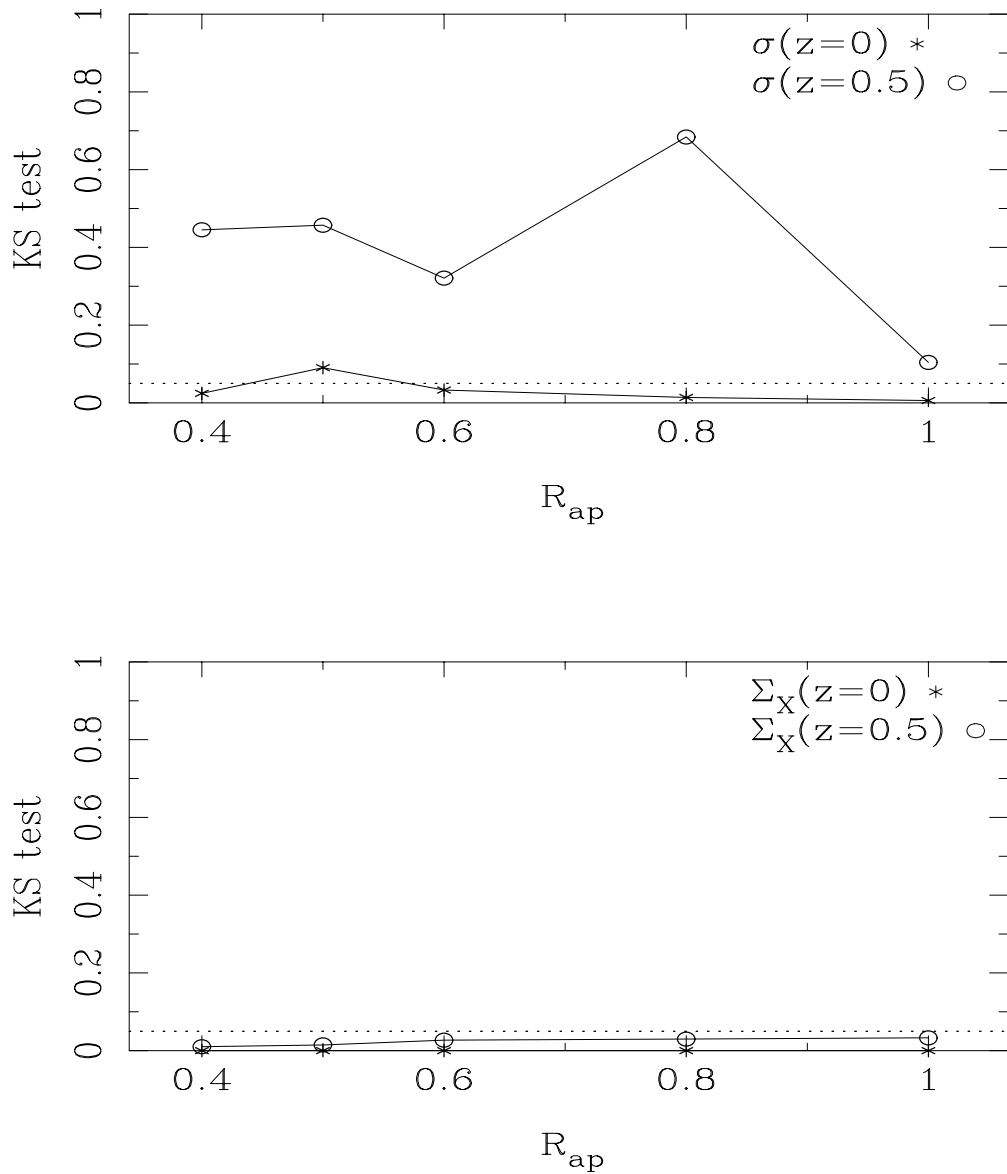


Fig. 4.— The same as Fig.3 but for  $P_2/P_0$ .

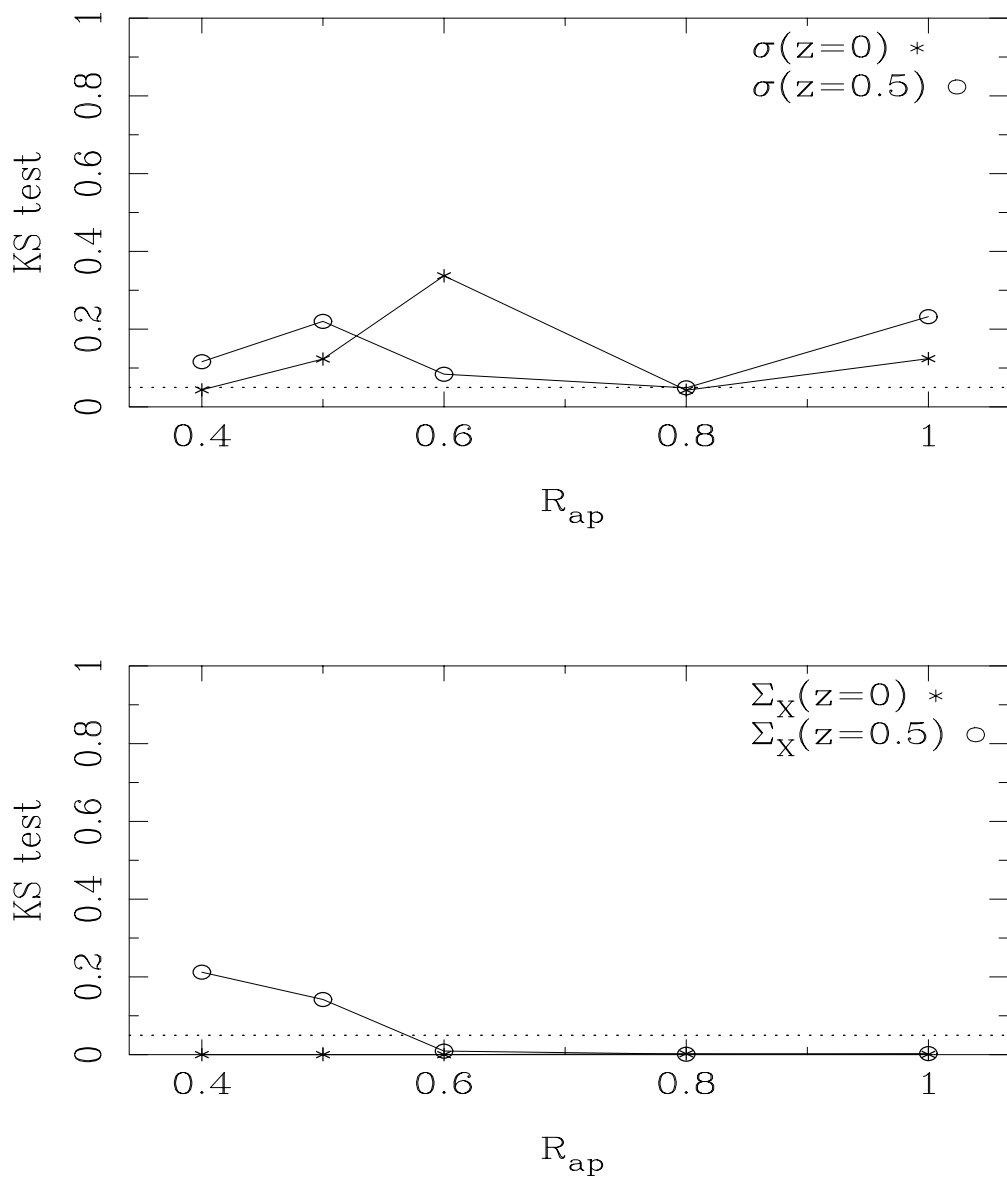


Fig. 5.— The same as Fig.3 but for  $P_3/P_0$ .

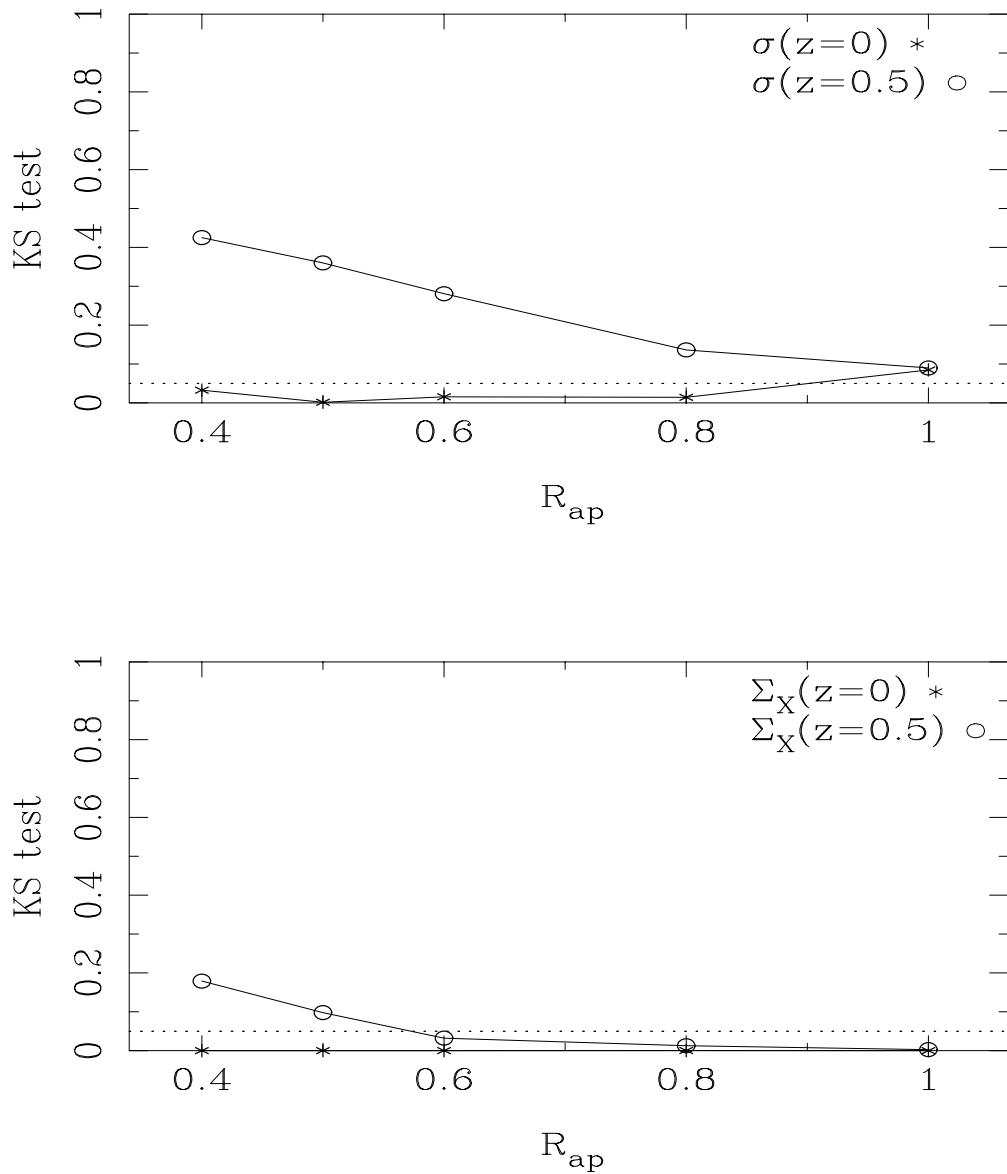


Fig. 6.— The same as Fig.3 but for  $P_4/P_0$ .

regions (i.e. in the central region) than those for  $\sigma$ , because  $\Sigma_X$  is proportional to square of gas density (and square root of temperature) as  $\rho_{\text{gas}}^2 T^{1/2}$ . Since small substructures which appear in the central region are expected to be erased more easily than large scale substructures, the power ratios for  $\Sigma_X$  are probably more sensitive to the cluster formation epoch than those for  $\sigma$ . In order to clarify this point we calculate power ratios for  $\sigma^2$ , and then perform KS-tests. The results for  $\sigma^2$  are better than those for  $\sigma$ , but worse than those for  $\Sigma_X$  reflecting the difference in relaxation time-scale. From these facts, we suggest that indicators that focus on the central regions of clusters are suitable to distinguish between  $\Lambda$ CDM and OCDM.

Some previous studies (Jing et al. 1995; Crone et al. 1996; Buote & Xu 1997) compared  $\Lambda$ CDM and OCDM by using pure N-body simulations in which they assume that  $\rho_{\text{gas}}$  is proportional to  $\rho_{\text{dm}}$ . For clusters which are not well relaxed, however, this assumption may not be valid. Using the power ratios for  $\Sigma_X$  Buote & Xu (1997) could not distinguish  $\Lambda$ CDM and OCDM, while we can. On the other hand, Jing et al. (1995) and Crone et al. (1996) showed that  $\Lambda$ CDM and OCDM are distinguishable by using center shifts, and we also reach the same conclusion. These results suggest that the power ratios are more sensitive to the existence of gas than the center shifts.

We shall discuss differences in the properties of these two indicators. The center shifts show a large value when there are substructures whose sizes are large enough to shift a center of contour from the inner contour to the outer one. Since the center shifts are sensitive to large size substructures that can be detected in the distributions of both gas and dark matter in the cluster, the center shifts for the simulations with and without gas are expected to be similar. In contrast, the power ratios are more sensitive to small size substructures than the center shifts and such small size substructures are sometimes detected in only the dark matter distribution since corresponding gas structures are already relaxed. Hence the difference between the power ratios for the simulations with and without gas is expected to be larger than that of the center shifts. In order to confirm this explanation, we calculate correlation coefficients of the power ratios for  $\Sigma_X$  and  $\sigma$ , and those of center shifts for  $\Sigma_X$  and  $\sigma$ . As expected, the correlation coefficients of the power ratios tend to be smaller than those of the center shifts. Therefore it is important to include a gas component in simulations in order to distinguish the two cosmological models using the power ratios.

Although some authors (Evrard et al. 1993; Mohr et al. 1995) employed gas particles, the number of clusters was too small (8 clusters for each model). We use much larger size simulations ( $L_{\text{box}} = 150h^{-1}\text{Mpc}$ ) than the previous studies in order to obtain a sufficient number of clusters to perform statistical tests (70–80 clusters at  $z=0$ ). The KS-test is significant when the number of samples is larger than 20 (Press et al. 1988).

Valdarnini et al. (1999) carried out hydrodynamic simulations for a sufficient number of clusters to perform statistical tests. By comparing their simulated clusters with ROSAT clusters, they showed that power ratios for gas in SCDM universes are in much better agreement with the ROSAT data than those for  $\Lambda$ CDM. Although this result is quite interesting, in order to give more conclusive results we should wait Chandra and XMM data which will be high resolution and high S/N and much higher resolution simulations with additional important physical processes such as radiative cooling, SNe feedback, and so on.

By comparison with the power ratios in  $\Lambda$ CDM obtained by Valdarnini et al. (1999), those obtained in this paper are systematically large. This difference results from the fact that the  $R_{ap}$  for our power ratios is proportional to  $r_{200}$ , while  $R_{ap}$  in their paper was constant. Thus, our power ratios are more sensitive to small-scale irregularity for small clusters than theirs. Mean values of power ratios and its standard deviations in our simulations agree well with their results for the constant  $R_{ap}$  case.

Schuecker et al. (2001) showed that the fraction of clusters of galaxies with substructures is almost 50% for REFLEX+BCS clusters after correction for several systematic effects. They also suggested that the fraction of clusters with substructures depends on the number density of the clusters. Then this large fraction may be explained by the fact that a large fraction ( $\sim 54\%$  for  $z \leq 0.1$ ) of rich clusters appear to belong to superclusters (Bahcall & Soneira 1984). On the other hand, the size of simulation box of our and previous simulations may not be large enough for the realization of large superclusters, such as the Shapley supercluster, since the Shapley supercluster is expected to be formed from a  $3.5\sigma$  perturbation with a size of  $\sim 30$ Mpc (Ettori, Fabian, & White 1997). This may be the reason why the previous simulations of open and flat  $\Lambda$  universes do not agree with the ROSAT X-ray observation data. We will simulate initial conditions corresponding to the local universe to examine this possibility.

Our conclusion is as follows. The power ratios and the center shifts for  $\Sigma_X$  can be used to distinguish between  $\Lambda$ CDM and OCDM. Since the formation histories of clusters in  $\Lambda$ CDM are similar to those in OCDM compared with the high-density universe, these indicators will be powerful probes to test the cosmological models in the non-linear regime.

We are grateful to Vincent Eke for helpful advice. We also thank the anonymous referee for valuable comments. Numerical computation in this work was carried out on the SGI Origin 2000 at the Division of Physics, Graduate School of Science, Hokkaido University, and on the VPP300/16R and VPP5000 at the Astronomical Data Analysis Center of National Astronomical Observatory, Japan.

## REFERENCES

Bahcall, N.A., Ostriker, J.P., Perlmutter, S., & Steinhardt, P.J. 1999, *Science*, 284, 1481

Bahcall, N.A., & Soneira, R.M. 1984, *ApJ*, 277, 27

Bertschinger, E. 1995, preprint (astro-ph/9506070)

Buote, D.A. 1998, *MNRAS*, 293, 381

Buote, D.A., & Tsai, J.C. 1995, *ApJ*, 452, 522

Buote, D.A., & Tsai, J.C. 1996, *ApJ*, 458, 27

Buote, D.A., & Xu, G. 1997, *MNRAS*, 284, 439

Clowe, D., Luppino, G.A., Kaiser, N., & Gioia, I.M. 2000, *ApJ*, 539, 540

Crone, M.M., Evrard A.E., & Richstone, D.O. 1996, *ApJ*, 467, 489

Davis, M., Efstathiou, G., Frenk, C.S., & White, S.D.M. 1985, *ApJ*, 292, 371

de Bernardis, P. et al. 2000, *Nature*, 404, 955

Dutta, S.N. 1995, *MNRAS*, 276, 1109

Ettori, S., Fabian, A.C., & White, D.A. 1997, *MNRAS*, 289, 787

Evrard, A.E., Mohr, J.J., Fabricant, D.G., & Geller, M.J. 1993, *ApJ*, 419, L9

Frenk, C.S., et al. 1999, *ApJ*, 525, 554

Gibson, B.K., et al. 2000, *ApJ*, 529, 723

Hernquist, L., & Katz, N. 1989, *ApJS*, 70, 419

Hockney, R.W., & Eastwood, J.W. 1981, *Computer Simulation Using Particle* (New York:McGraw Hill)

Jing, Y.P., & Fang, L.Z. 1994, *ApJ*, 432, 438

Jing, Y.P., Mo, H.J., Börner, G., & Fang, L.Z. 1995, *MNRAS*, 276, 417

Luppino, G.A., & Kaiser, N. 1997, *ApJ*, 475, 20

Mellier, Y. 1999, *ARA&A*, 37, 127

Mohr, J.J., Evrard, A.E., Fabricant, D.G., & Geller, M.J. 1995, *ApJ*, 447, 8

Monaghan, J.J. 1992, *ARA&A*, 30, 543

Perlmutter, S., et al. 1999, *ApJ*, 517, 565

Press, W.H., Flannery, B.P., Teukolsky, S.A., & Vetterling, W.T. 1988, *Numerical Recipes in C* (Cambridge: Cambridge Univ. Press)

Richstone, D., Loeb, A., & Turner, E.L. 1992, *ApJ*, 393, 477

Riess, A.G., et al. 1998, *AJ*, 116, 1009

Schneider, P., & Bartelmann, M. 1997, *MNRAS*, 286, 696

Schuecker, P., Böhringer, H., Reiprich, T.H., & Feretti, L. 2001, *A&A*, 378, 408

Thomas, P.A., et al. 1998, *MNRAS*, 296, 106

Totani, T. & Kobayashi, C. 1999, *ApJ*, 526, L68

Tsai, J.C., & Buote, D.A. 1996, *MNRAS*, 282, 77

Valdarnini, R., Ghizzardi, S., & Bonometto, S. 1999, *New Astron.*, 4, 71

Wilson, G., Cole, S., & Frenk, C. S. 1996, *MNRAS*, 282, 501

Yoshikawa, K., Jing, Y.P., & Suto, Y. 2000, *ApJ*, 535, 593